Journal of the European Ceramic Society 21 (2001) 389–397

www.elsevier.com/locate/jeurceramsoc

How the trapping of charges can explain the dielectric breakdown performance of alumina ceramics

J. Liebault [a], J. Vallayer [b], D. Goeuriot [a,*], D. Treheux [b], F. Thevenot [a]

[a] *Ecole Nationale Supérieure des Mines de Saint-Etienne, Departement Céramiques Spéciales, F-42023 St-Etienne cedex 2, France*
[b] *Ecole Centrale de Lyon, UMR 5621, Ingéniérie et Fonctionnalisation des Surfaces, BP163, F-69131 Ecully cedex, France*

Received 14 September 1999; received in revised form 10 June 2000; accepted 17 June 2000

Abstract

The aim of this work is to bring new elements to the understanding of breakdown phenomena. Different alumina materials are studied in breakdown tests and by absorbed current measurement. The association of these two characterisation methods displays correlations between breakdown strength, the ability to trap or diffuse electrical charges and microstructural parameters. Different materials have been studied with a growing quantity of defects: structural defects in the single crystal, grain boundaries in very pure polycrystalline alumina (99.99%), impurities in less pure polycrystalline alumina (99.8%), interfaces in the case of alumina with a dispersion of zirconia and finally the adding of sintering aids. It appears that materials capable of diffusing injected charges have higher breakdown values than those trapping charges locally. Two other favourable behaviours are characterized: trapping charges at the injection point in order to limit the injection process, and trapping followed by reemission which relaxes the insulator and delays breakdown.

Keywords: Al_2O_3; Dielectric properties; Dielectric breakdown; Impurities; Insulators

1. Introduction

The dielectric properties of insulators, and specially dielectric strength, strongly depend on defects. Defects are considered as sites where polarizability is modified and where charge and energy localisation can occur. [1–4] In ceramics, such defects can comprise porosity, crystallographic defects, lattice distortions, impurities, grain boundaries or interfaces with a secondary phase.

In this work, a correlation is proposed between breakdown events, defects in alumina materials and the trapping of charges. The nature of the defects is controlled in ascending severity from sapphire samples to sintered polycrystalline alumina with various purity contents and grain sizes. The effect of porosity has been discussed before.[5] It was demonstrated for alumina materials that breakdown strengths vary from 6 to 13 kV/mm while the porosity varies from 15 to 5%. If the porosity is lower than 5%, then the breakdown strength remains constant (at ± 0.5 kV/mm). As most of the samples considered have a low content of pores (< 5%), it will be assumed that residual porosity has relatively little influence on the dielectric properties.

2. Experimental

2.1. Materials

Slices of single crystal (A) were taken from a Verneuil-grown sapphire rod provided by Rubis Synthéthique des Alpes (France). They were polished and heated to 1500°C for 4 hours to eliminate stresses and to remove any defects induced by the machining. Defects are then principally oxygen vacancies and impurities.[6] Their impurity contents are noted in Table 1. The great amount of SiO_2 is suspected of coming from an error of analysis. Single crystals are indeed elaborated from pure alumina powder like E0 and should present the same impurity contents.

* Corresponding author.
E-mail address: dgoeurio@emsc.fr (D. Goeuriot).

0955-2219/01/$ - see front matter
PII: S0955-2219(00)00186-2

Table 1
Characteristics of alumina materials

Ref.				Impurity (ppm)				
				SiO_2	CaO	MgO	Na_2O	Fe_2O_3
Single crystal		A		620	22	< 16	26	69
Polycrystalline alumina	99.99%	E0		90	5	< 5	40	12
		Doped	EMg	143	28	675	31	20
			ECa	86	480	< 5	11	9
	99.8%	B1		1497	686	723	404	415
		B2		1070	389	693	539	313
	Addings	B2 + 5 vol.% ZrO_2		B2 alumina + 7.8 mass% ZrO_2 (%)				
		C1		2.10	2.08	–	0.18	< 0.01–
		C2		4.63	0.46	1.56	0.15	0.04

In order to introduce grain boundaries, polycrystalline alumina samples were prepared from the alumina powder E0 with the same purity (EXAL process) (Table 1). As the sintering temperatures are close to 1500°C, it can be supposed that the nature and distribution of point defects in each grain of polycrystalline alumina are not far from those in sapphire. However, the probability to have a segregation of impurities at grain boundaries must not be omitted.

This type of material was then further complicated by the addition of two of the elements frequently met in alumina ceramics, calcium and magnesium. Powder EMg was industrially doped with 675 ppm MgO and powder ECa was obtained by a doping of E0 with 480 ppm CaO based on the addition of water soluble $Ca(NO_3)_2$ (Table 1). Good dispersion of Ca was not obtained and the sintered samples presented inhomogeneous grain size.

Other kinds of polycrystalline alumina samples were sintered with various impurity contents (notably Si) and grain sizes using powders issued from the BAYER process (Table 1). The main difference between powders B1 and B2 is a greater content of Si and Ca for B1.

It can be noted that, to control the sintering parameters (density, grain size), powders were prepared according to definite procedures using aqueous dispersion, adding of organic binders, spray drying, and cold isostatic pressing. Sinterings were all performed in air. Then various microstructures were obtained with controlled sintering routes. Applied pressures (cold) varied between 137 and 400 MPa, sintering times between 90 min and 6 h, and sintering temperatures between 1450 and 1650°C.

In a last part, more complex systems were considered: alumina ceramics with 5–8% of addition phases. First, alumina–5 vol.% zirconia composites have been synthesized and characterized to show the influence of dielectric interfaces. Zirconia has been selected for its high dielectric permittivity ($\epsilon_r \sim 30$ compared to ~ 10 for alumina); this should modify charge transport by creating deep trapping sites.[7] Composites were prepared by mixing alumina and zirconia powders in aqueous conditions. ZrO_2 powder (6–8 m^2/g) was stabilized by Y_2O_3 addition (3 mol%) and after sintering, the zirconia grains are only intergranular.

Finally, commercial alumina ceramics with 5–8% of sintering aids (C1, C2, Table 1) were investigated to study the influence of secondary phases in alumina grain boundaries, containing a great amount of SiO_2, CaO and MgO. These materials present more irregular microstructures. Mean grain size is around 3–5 μm for C1 samples and 7–10 μm for C2 samples compared to 1–2 μm homogeneous grain size for pure alumina. Porosity is also more important and can reach 10 μm in diameter in the case of C2.

Samples are generally polished and annealed in air (1200°C/3 h for polycrystals) to minimize defects due to polishing. It should be remarked that heat treatment at 1200°C on alumina C1 and C2 induced changes in surface composition. There was crystallisation of new phases as shown in Table 2, and these samples were considered as new materials. Another range of heat treatment (900°C/2 h) was needed to preserve the initial compositions from other samples.

2.2. Breakdown tests

Breakdown concerns dielectric materials submitted to high tensions. This phenomenon corresponds to the loss

Table 2
Characteristics of C1 and C2 samples surface after heat treatments at 900 and 1200°C[a]

	XRD (surface analysis)		
	Unpolished	HT 900°C	HT 1200°C
C1	Vitreous	ϵ (A, G)	A, G
C2	Vitreous	Vitreous	A, S, C, Ca_2Si

[a] A, anorthite, $Al_2O_3.2SiO_2.CaO$; G, gehlenite, $Al_2O_3.SiO_2.2CaO$; S, spinel, $MgAl_2O_4$; C, cordierite, $2MgO.2Al_2O_3.5SiO_2$.

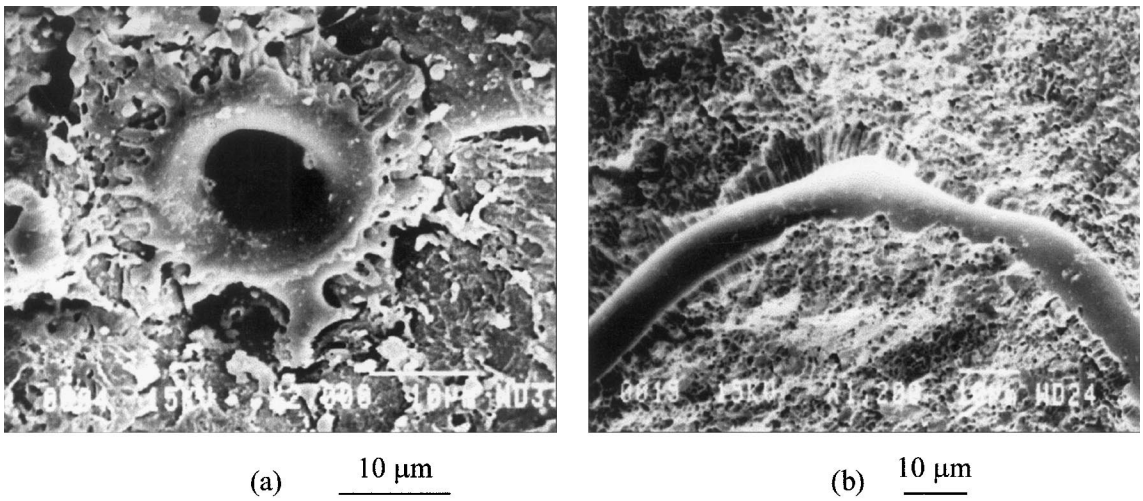

Fig. 1. Perforation of an alumina sample after breakdown test: (a) SEM observation of the crater appeared on the surface of the material; (b) SEM observation of the channel crossing the insulator.

of insulating properties and mechanical degradation of the material. Fig. 1 shows the perforation of an alumina sample (crater and channel) caused by the flow of a breakdown current. Insulators are characterized by a breakdown strength, E_b, defined as the maximum tension value obtained before the onset of current.

Bulk breakdown tests were performed on cylindrical samples of 20 mm in diameter. As the breakdown strength, E_b, strongly depends of sample thickness, all the samples were approximately 3 mm thick. Having determined the evolution law of E_b in the range of 0.7–3.5 mm for this type of materials, each value of E_b was calculated for a thickness of 3 mm exactly. In this condition, all E_b values are strictly comparable, and calculated from the expression: $E_b = V_b/t = A.t^{-0.5}$, with V_b tension measured when breakdown occurs (kV), t, sample thickness (mm), and A, characteristic constant of the material.

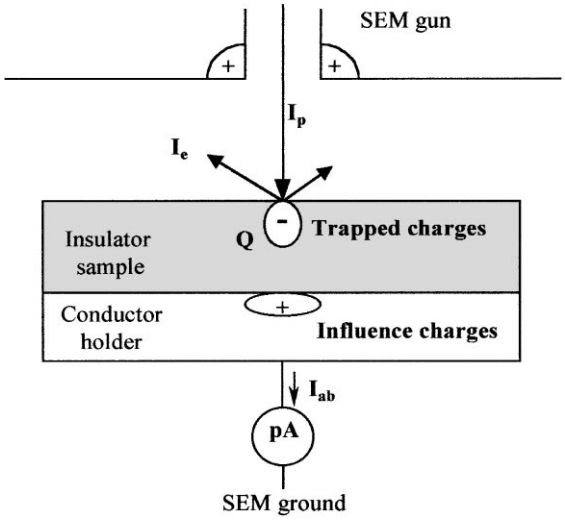

Fig. 2. Injection of electrons and absorbed current measurement using a SEM: I_p, primary electron beam; I_e, secondary electron emission; Q, trapped charges; I_{ab}, absorbed current.

The test procedure must be precise enough to reduce the dispersion of E_b values. Specimens were tested directly after sintering to avoid surface impurities. Each sample was clamped between a pair of hemispherically ended brass electrodes. The entire system bathed in transformer oil to avoid flashover behaviour. After specimen immersion, the oil bath was stirred with a magnet during 1 minute to evacuate bubbles, and was then left for 1 minute without moving before the voltage rise in order to stabilize the environment of the sample. The dielectrimeter (DieltestDTS-BAUR) operated on alternative current (50 Hz) at room temperature. The voltage rose at a rate of 1 kV/s until the insulator underwent breakdown. About 15 values of breakdown voltage were needed to have an average breakdown strength E_b (kV/mm). These 15 values were obtained by testing five specimens of each type with three separated impacts for each specimen.

In these conditions, the standard error was mainly around 0.5 kV/mm and so, results can be only discussed in terms of the mean value.

2.3. Trapping of charges

The possibility to create trapped charges in ceramics can be measured experimentally using a Scanning Electron Microscope equipped with a cold-hot stage (see the "SEM Mirror effect method" in Refs. 8 and 9).

During electron injection using the SEM electron beam at high energy (few 10 kV), the secondary electron emission yield δ is less than 1. Then negative trapped charges, Q, appear in the insulating material which produce positive "influence" charges in all conductor pieces of the SEM chamber (mainly in the holder and gun) (Fig. 2).

Table 3
Microstructural characteristics and breakdown strengths of pure polycrystalline alumina (E0) compared to single crystal (A)

Ref.	Density d (%)	Average grain size Φ (μm)	Breakdown strength E_b (kV/mm)
A	–	–	13.07±1.34
E0-1	97.4	1.2	14.82±0.81
E0-2	98.3	1.1	15.50±0.50
E0-3	98.9	2.7	15.23±1.15

We consider that electrons conducted through the insulator to the holder are negligible and consequently the absorbed current (I_{ab}) measured between the holder and the ground is only produced by the influence charges. I_{ab} is directly proportional to the quantity of trapped charges: $dQ/dt = \alpha\ I_{ab}$, where α is a factor depending on the geometric configuration of the experimental set-up ($\alpha \geqslant 1$).[10]

Consequently the evolution of the absorbed current measured during injection gives information on the different steps of trapping and furthermore on the localisation or the diffusion of charges in the dielectric when observing the first moment of injection.

After injection, the observation of the sample surface at low accelerating voltage of electrons (few 100 V) can reveal "a mirror effect"[8,9] if the trapped charge Q is sufficiently concentrated to create an electric field strong enough to deflect the incoming electrons, as a convex mirror with light. This mirror effect gives complementary information on the density of trapped charges.

Before testing, each sample is annealed at 300°C for 3 h in vacuum inside the SEM chamber to avoid surface contamination. Injections of electrons were performed at room temperature to correlate the observations to breakdown results. Conditions of charge injection have been optimised to a current of 3 nA during 100 ms, with a focused electron beam of 30 keV. In this conditions, the quantity of injected charges was equivalent to 300 pC.

Finally, as our materials present random position of defects (pores, grain boundaries, impurities, defects due to polishing), 15 injections, equally spaced every 2 mm, were needed to have a statistical view of the behaviour of each sample.

3. Results and discussion

3.1. From single crystal to pure polycrystal

As reported in Table 3, single crystals have a lower breakdown strength than polycrystalline samples with average grain size between 1 and 3 μm. In absorbed current measurements, variations are clear between sample E0-2 and sapphire (Fig. 3).

For sapphire (Fig. 3a), the current variation is characterized by a strong decrease after the starting injection. This behaviour is associated with localisation of charges. The high concentration of trapped electrons at the injection point constitutes an electrostatic barrier for the primary electrons, injection is momentarily compromised and the current falls. After the injection, a mirror effect is observed which is consistent with the point localisation of charges.

Absorbed current measurement for the pure polycrystal sample shows a high level for the first value (Fig. 3b). The material absorbs a great quantity of charge. These charges spread sufficiently to avoid a rapid decrease of the current. So the great quantity of charge injected is not trapped at the injection point but diffuse into the solid. This ability to diffuse charges can be here attributed to the presence of grain boundaries. Despite the possibility to have a segregation of impurities, grain boundaries offer a more favourable state than a single crystal with a higher dispersion of impurities.

Moreover, it can be noted that by using the SEMM method, no "mirror" effect has been observed for polycrystalline alumina, even at low temperature when energy activation is large. Diffusion occurs and the

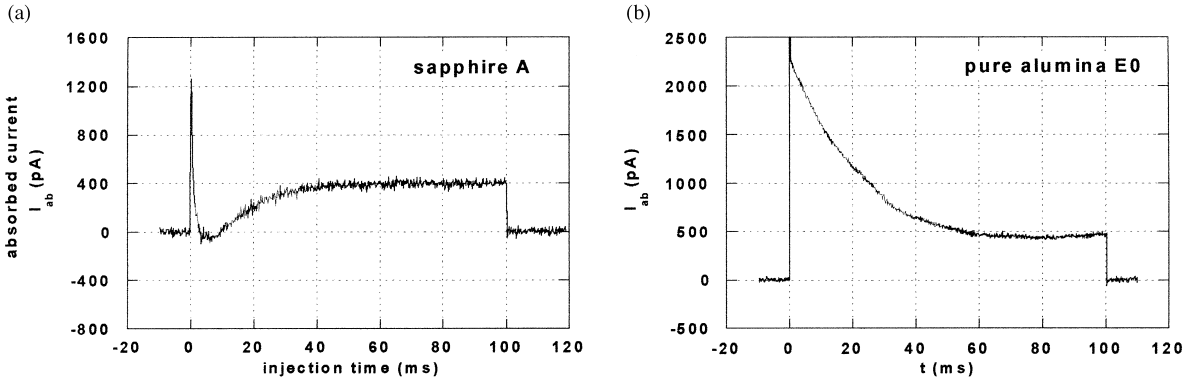

Fig. 3. Absorbed current variations for (a) single crystal A and (b) pure polycrystalline alumina E0 (sample E0-2), at 25°C.

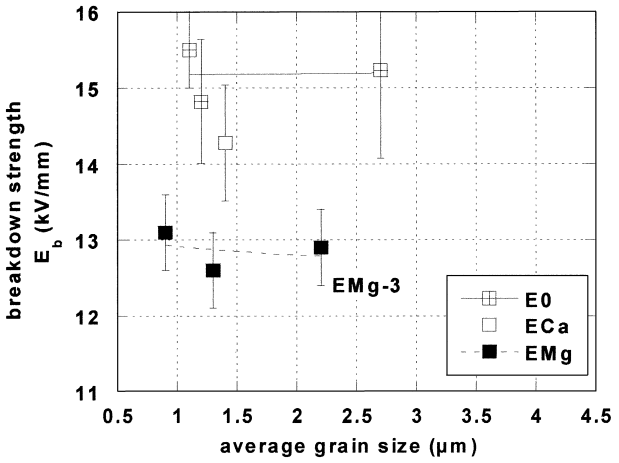

Fig. 4. Breakdown strength evolution with alumina grain size for pure alumina E0, Ca- and Mg-doped aluminas.

density of charges is not sufficiently important to induce such an effect.

According to these results, it can be said that diffusion of electrons along grain boundaries avoids concentration of charges and induces higher breakdown strengths.

3.2. Effect of CaO and MgO doping

According to the dispersion of E_b values, addition of nearly 500 ppm CaO in pure alumina E0 has no influence on breakdown (14.3±0.8 compared to 15.2±0.5 kV/mm). But the presence of MgO decreases E_b from 15 to 13 kV/mm (Fig. 4).

Absorbed current variation for the ECa sample (density d= 97.4%, average grain size Φ= 1.4 μm) is not very different from pure alumina (d= 98.3%, Φ= 1.1 μm) with a diffusion of injected charges [Fig. 5a, ECa-(1)]. The main difference lies in the non-reproducibility. Three measures out of fifteen show a current decrease at the starting injection [ECa-(2)]. This type of material presents a worse homogeneity and there are structural parameters which keep the charges localised. The bad dispersion of CaO favours the formation of calcium aluminates in the alumina grain boundaries. These randomly dispersed secondary phases should be the cause of the light change of dielectric behaviour of alumina.

Concerning the EMg-3 sample (Fig. 4), the average grain size is not so far from that of previous samples (~2 μm). Absorbed current variations are characterized by an instantaneous decrease at the beginning of injection (Fig. 5b). Electrons are locally trapped and constitute a local barrier for the primary electrons. After this short first step, competition between injection and electronic emission is restored leading to constant injection. This tendency to keep charges localised is then associated with bad results in breakdown tests. According to the doping rates and the solubility of Mg in alumina (~150 ppm, 1560°C[11]), we can consider that only a fraction of this element is dissolved in the alumina matrix, and the observed dielectric behaviour can be attributed to the presence of the spinel phase $MgAl_2O_4$ in the alumina grain boundaries.

3.3. 99.8% pure aluminas

The two alumina B1 and B2 are described in Table 1. Samples were sintered in order to obtain different grain sizes. The notation is $Bx-y$, with x= 1 or 2, depending on the alumina powder and y, the average grain size.

Here, the breakdown strengths are lower than those of very pure alumina and decrease when grain size becomes larger (Fig. 6) (standard error 0.5 kV/mm). Moreover, these polycrystalline aluminas present several types of breakdown evolution according to impurity content. The decrease with grain size is faster for alumina B2 which has lower Si and Ca contents.

In order to correlate these behaviours to the trapping of charges, two values of average grain size have been selected: 1 and 2 μm. For samples B1-1 (d=95.7%, Φ=1.2 μm) and B2-1 (d= 97.4%, Φ= 1.1 μm) (Table 1), the fine grain size obtained provides a high density of

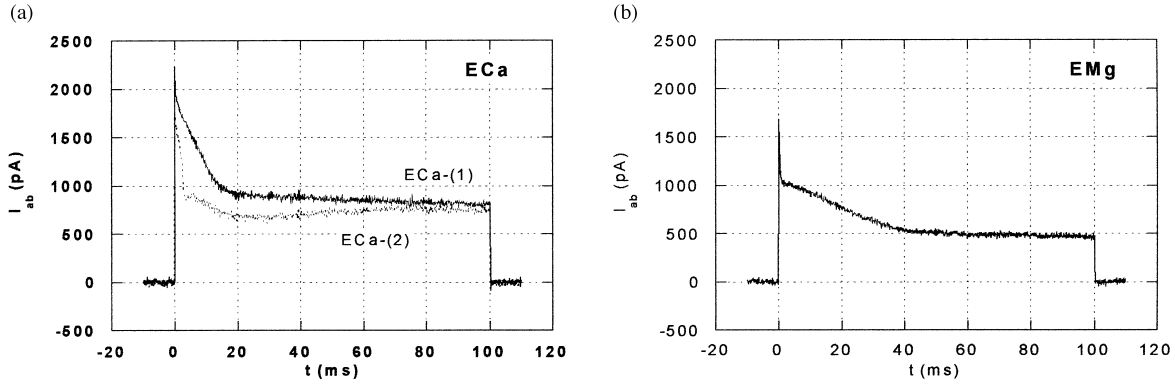

Fig. 5. Absorbed current variations for (a) Ca- and (b) Mg-dopped aluminas at 25°C: ECa-(1), major evolution, ECa-(2), three current evolutions measured on 15.

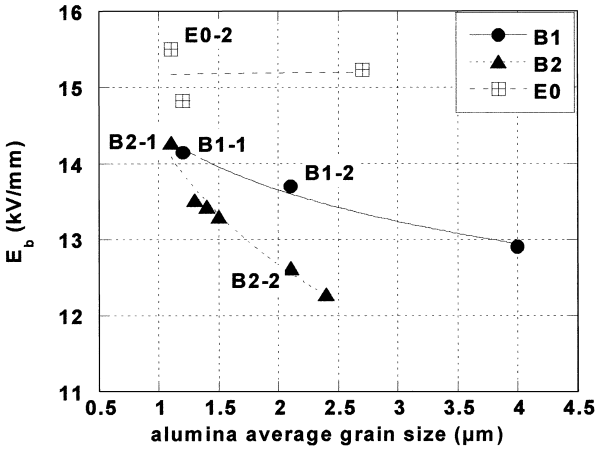

Fig. 6. Breakdown strength evolution with grain size for 99.8% pure aluminas B1 and B2 compared to 99.99% pure alumina E0.

grain boundaries and good dispersion of impurities in the grain boundary. They have the same breakdown strength (E_b~14.2 kV/mm) and absorbed current measurements show the same constant evolution (Fig. 7a and b). Charges are immediately diffused and injection progresses continuously during all the injection time. This interpretation is supported by the absence of any mirror effect after injection.

However, when the grain size becomes larger, the breakdown strength of alumina B2 (B2-2 sample, d=99.2%, Φ=2.1 μm) falls down to 12.5 kV/mm compared to 13.7 kV/mm for alumina B1 (B1-2 sample, d=98%, Φ= 2 μm). For both samples, absorbed current variations show localisation of charges at the starting injection, but different behaviours in the following injection times (Fig. 7c and d). Localisation in the case of B1 seems to limit the injection of new electrons and the current stays near zero. For B2, absorbed current becomes negative that means the emission of electrons is important, and then injection starts again and the current increases. More effective charges are injected and trapped into the material, and breakdown performance is lowered.

The different microstructures were obtained with similar sintering temperatures and it can be considered that as the number of grain boundaries decreases when the grain size increases, impurity concentration and so the nature and the quantity of secondary phases in the grain boundary are not the same. Still here, the nature of grain boundary seems to predominate. So, even for this kind of material considered as pure alumina, the distribution and the proportion of impurities in the grain boundary have a strong influence on the dielectric properties.

3.4. Alumina–zirconia composites

Samples synthesized by well-controlled powder mixing were characterized by a good repartition of fine

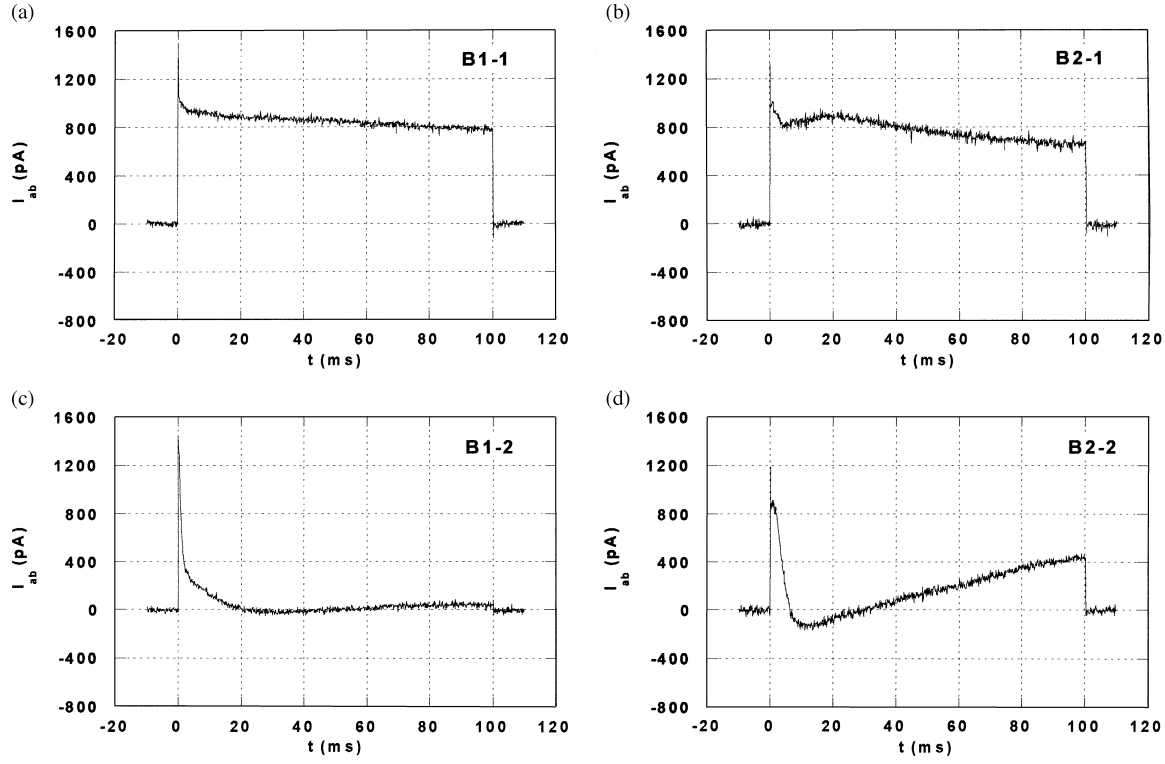

Fig. 7. Absorbed current variations for two grain size families of B1 and B2 aluminas: (a) and (b): fine grains (~1 μm); (c) and (d): large grains (~2 μm).

grains of Al_2O_3 and ZrO_2. In Fig. 8, E_b values are represented as a function of the mean grain size.

The results concern samples with homogeneous structure characterized by fine grains of Al_2O_3 (1–2 μm) and ZrO_2 (<0.5 μm) (Fig. 9). The zirconia phase is present in intergranular position and, according to X-rays diffraction analysis, the monoclinic transformation rate is low whatever the preparation route. E_b values are better than for pure alumina, and the evolution with alumina grain size is nearly the same. So the presence of zirconia in the alumina grain boundaries transfers breakdown results to higher values. Such microstructures prove the interest of using ZrO_2 dispersion in alumina ceramics to improve breakdown strength.

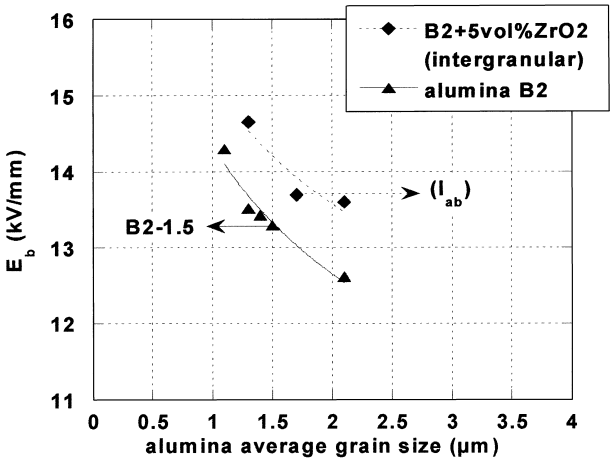

Fig. 8. Breakdown strengths of alumina–zirconia composites compared to pure alumina B2, in function of alumina grain size (points in evidence will be studied by the absorbed current measurement).

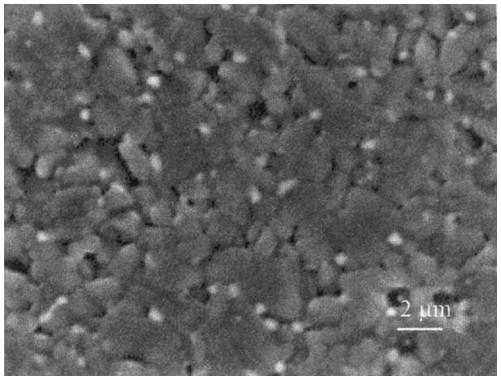

Fig. 9. Scanning electron micrographs of Al_2O_3/5 vol.% ZrO_2 composites: intergranular ZrO_2.

Absorbed current measurement was performed on one sample with a 1.7 μm average alumina grain size (d=95.7%). Current variations look like those of fine grain alumina (B2-1 sample, cf. Figs. 6 and 7b) with a constant injection that proves good diffusion of injected charges (Fig. 10a). In the pure alumina B2 with the same average grain size (B2-1.5 sample, d=98.7%, Φ=1.5 μm, Fig. 8), without the intergranular zirconia grains, the absorbed current decreases instantaneously after the starting injection (Fig. 10b). So, when the zirconia grains are present in the alumina grain boundaries, the phenomena of localisation of charges disappear.

From this short analyse, it can be said that when having a good dispersion of fine intergranular zirconia grains in alumina, the nature of the grain boundary is modified with the result that charges are progressively diffused in the material and the breakdown strength is improved.

3.5. Alumina with 5–8% of sintering aids

The complexity and the non-homogeneity of these microstructures induce higher dispersion in breakdown results as in absorbed current measurements. Moreover, the behaviours of alumina samples C1 and C2 are highly dependent on the temperature treatments.

After treatment at 900°C, alumina C1 has the higher breakdown strength (Fig. 11). The major absorbed current evolution [(C1-(1)] shows a localisation of charges which limits injection (Fig. 12a). Other local responses [C1-(2)] display the capacity to diffuse charges. These two kinds of behaviour agree with the high breakdown strength obtained in B-samples.

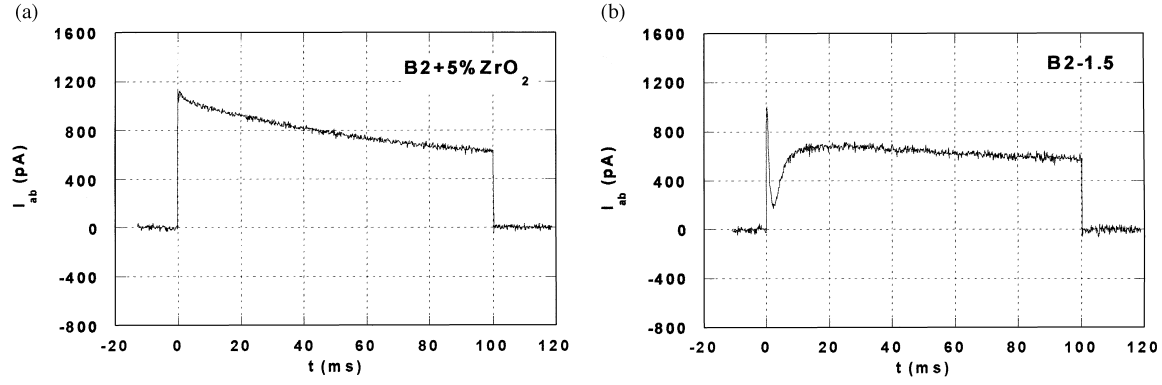

Fig. 10. Absorbed current variations for a B2+5% ZrO2 sample presenting high E_b compared to pure alumina B2 with nearly the same alumina average grain size.

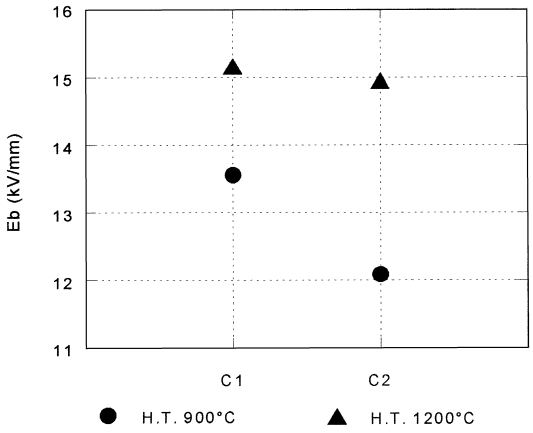

Fig. 11. Breakdown strengths of C1 and C2 alumina materials according to the two heat treatments at 900 and 1200°C.

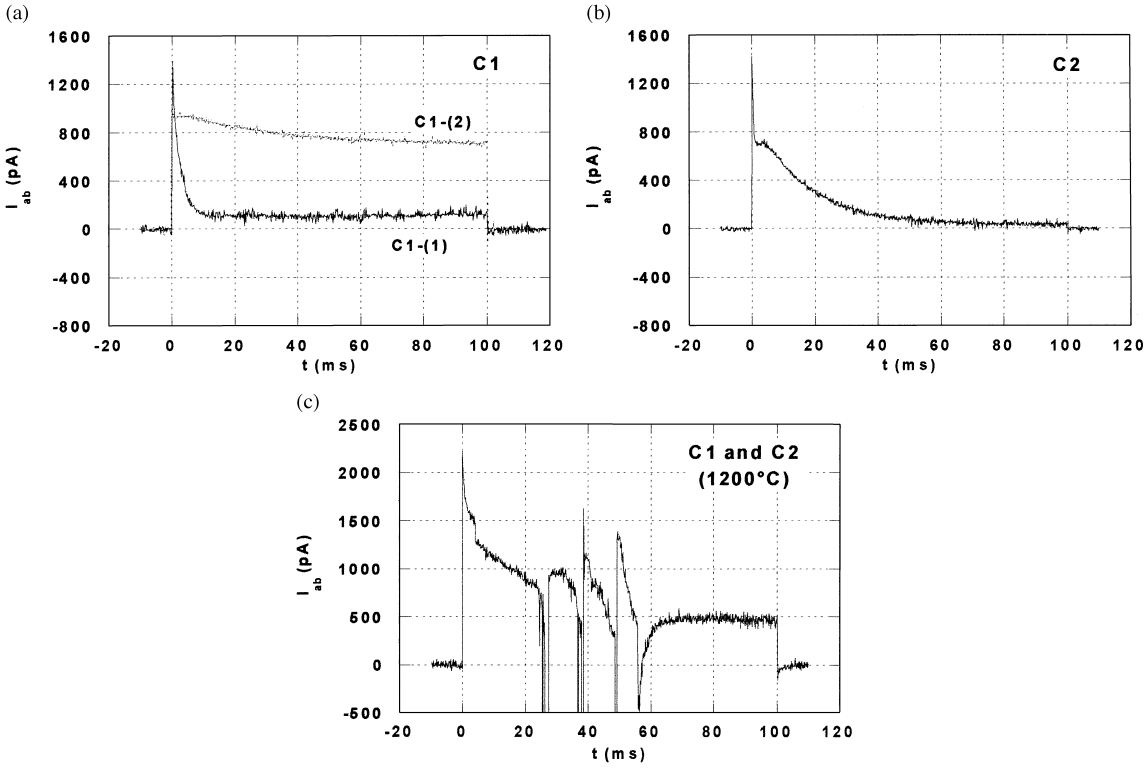

Fig. 12. Absorbed current variations for (a) C1 and (b) C2 alumina materials after heat treatment at 900°C and (c) after heat treatment at 1200°C [C1-(1), major evolution; C1-(2), 2 measures on 15].

In contrast, the absorbed current of the C2 sample is typical of a greater quantity of trapped charges, based on the recovery of injection (Fig. 12b). This behaviour causes a premature breakdown.

So, it seems that the alumina with the finest microstructure has the best behaviour. Having fine grains, low porosity, absence of Mg, and a low impurity content seems to be favourable to accommodate charges in excess and to improve breakdown strengths. But such systems are too complex to determine what phases are favourable or not. These two examples show the importance of vitreous or partially crystallized secondary phases and the probability to have balanced effects between the different microstructural parameters.

After treatment at 1200°C, these two aluminas have nearly the same E_b value, and higher than in the previous case (Fig. 11).

When regarding absorbed current variations, there is new behaviour characterized by frequent current oscillations (Fig. 12c). Here, the materials trap a certain quantity of charges until electronic reemission happens instantaneously. Then injection is recovered and so on. In these cases, vitreous or partially crystallized phases developed at the sample surface have a high ability to

trap charges. They constitute a barrier which keeps and emits electrons. The whole material is then guarded from injection of more charges and the breakdown strength is really improved. In our conditions of test, the two materials become then equivalent.

4. Conclusion

In our conditions of test, the alumina materials studied here present breakdown strength differences with often small differences in microstructure and despite the important dispersion of this type of characterization test. Absorbed current measurement gives complementary information on the insulator response to the injection of electrons. The fact that some materials, having different microstructures, could have the same breakdown strength can be explained by the ability to keep trapped charges localized or to diffuse them. Correlation with structural elements can be then developed even if more cautiously. Finally, three main behaviours are associated to breakdown improvement:

i. diffusion of charges: the absorbed current does not show an important decrease after the starting injection. Here its evolution with time is light and constant (B1-1 sample), and no mirror effect can be observed.

ii. trapping limiting injection: the current variation is characterized by a strong decrease after the starting injection, followed by a constant and low level (B1-2 and C1-1 variations). There is no mirror effect.

iii. trapping in surface phases with instantaneous electron reemission: the current is characterized by several peaks which correspond to an important electronic reemission. The frequency of these peaks depends on the studied material (nature of surface phases).

Acknowledgements

The authors thank Janick Bigarré and Denyse Juvé of Ecole Centrale de Lyon for technical collaboration for the SEM equipment and for helpful discussions.

This work is a part of the PhD thesis of J. Liebault, "Comportement d'alumines face à l'injection des charges. Relations microstructure-claquage diélectrique-mesure des charges d'influence (méthode SEMM)", Ecole Nationale Supérieure des Mines de Saint-Etienne, no. 206 TD, February 1999.

References

1. Le Gressus, C. and Blaise, G., Insulator damages related to charge detrapping. In *Conference on Electrical Insulation and Dielectric Phenomena Proceedings*, 1993, pp. 574–577.
2. Blaise, G., Charge trapping/detrapping induced lattice polarization/relaxation processes, In *CEIDP Proceedings*, IEEE Annual Report, 1995, pp. 37–39.
3. Blaise, G., Fields and polarisation, conduction and charge trapping in insulating materials. In *CSC'3 Proceedings*. SFV, 1998, pp. 25–37.
4. Moya-Siesse, D., Moya, G. and Le Gressus, C., Energy released during space charge relaxation induced breakdown. In *CEIDP Proceedings*, 1993, pp. 146–149.
5. Liébault, J., Bigarré, J., Tréheux, D., Goeuriot, D. and Thévenot, F., Influence of microstructural parameters on dielectric properties of polycrystalline alumina. In *CSC'3 Proceedings*, SFV, 1998, pp. 391–400.
6. Jardin, C., Durupt, P., Bigarré, J. and Le Gressus, C., The surface potential and defects of insulating materials probed by electron and photon emissions. In *CEIDP Proc., IEEE Annual Report*, 1995, pp. 548–551.
7. Bigarré, J., Fayeulle, S. and Tréheux, D., Application of the mirror method to the study of chromium doped and zirconium ion implanted sapphire, In *CEIDP Proc., IEEE Annual Report*, 1995, pp. 676–679.
8. Damamme, G., Le Gressus, C. and De Reggi, A. S., Space charge characterization for the 21th century. *IEEE Trans. on Dielectrics and Electrical Insulation*, 1997, **4**(5), 558–584.
9. Vallayer, B., Blaise, G. and Tréheux, D., Space charge measurement in a dielectric material after irradiation with a 30 kV electron beam. In *Review of Scientific Instruments*, 1999, **70**(7), 3102–3112.
10. Berroug, A., Bigarré, J., Fayeulle, S. and Tréheux, D., Charging effects under electron beam injection on sapphire implanted with Zirconium ions. In *CEIDP Proc., IEEE Annual Report*, 1997, pp. 97–100.
11. Roy, S. K. and Coble, R. L., Solubilities of magnesia, titania and magnesium titanate in aluminium oxide. *J. Am. Ceram. Soc.*, 1968, **51**(1), 1.